Research Article

Nano Research
2023, 16(7): 10272–10278

ISSN 1998-0124 CN 11-5974/O4
https://doi.org/10.1007/s12274-023-5724-9

Gap-surface-plasmon induced polarization photoresponse for MoS_2-based photodetector

Qinghu Bai[1,2,§], Xin Huang[1,2,§] (✉), Yang Guo[1,2], Shuo Du[1,2], Chi Sun[1,2], Leyong Hu[1,2], Ruixuan Zheng[1,2], Yang Yang[1], Aizi Jin[1], Junjie Li[1,3], and Changzhi Gu[1,2] (✉)

[1] *Beijing National Laboratory for Condensed Matter Physics, Institute of Physics, Chinese Academy of Sciences, Beijing 100190, China*
[2] *School of Physical Sciences, CAS Key Laboratory of Vacuum Physics, University of Chinese Academy of Sciences, Beijing 100190, China*
[3] *Songshan Lake Materials Laboratory, Dongguan 523808, China*
[§] *Qinghu Bai and Xin Huang contributed equally to this work.*

Received: 10 February 2023 / **Revised:** 26 March 2023 / **Accepted:** 9 April 2023

ABSTRACT

Polarization-sensitive photodetectors based on two-dimensional (2D) materials have shown more attractive application prospects compared to traditional thin-film photodetectors due to their atomic thickness, tunable bandgap, high mobility and strong light–matter interactions. Among them, 2D molybdenum disulfide (MoS_2) has drawn numerous attentions in photodetection due to its wide spectral range, remarkable photoresponsivity and fast photo-switching rate. However, the isotropic crystal structure of MoS_2 hampers its application in the polarization-sensitive detection, which is highly desired in military and civilian applications. In this paper, we demonstrated an integration of plasmonic nanocavity with monolayer MoS_2 to achieve high photoresponsivity and polarization-sensitive photodetector. With the significant enhancement of electromagnetic field provided by the gap-surface-plasmon (GSP), we achieved a significant photoluminescence (PL) enhancement of 24-fold. Relying on the enhanced light absorption by our plasmonic nanocavity, which generally facilitates photo-generation of electron–hole pairs in MoS_2, we achieved a high photoresponsivity of 1.88 A/W and degree of linear polarization (DOLP) of 0.8 at the excitation wavelength of 633 nm. Our work provides a feasible and universal solution to realize polarization-sensitive photodetector of MoS_2 for high-performance and polarization-sensitive photodetectors.

KEYWORDS

gap-surface-plasmon, nanocavity, MoS_2, photodetector, linear polarization

1 Introduction

The main physical parameters of a light wave contain amplitude, phase, frequency, and polarization. Beyond conventional amplitude and frequency photodetection, the ability to obtain the optical polarization by linearly polarized photodetection extremely expands the capabilities of numerous applications, such as remote optical sensing, biomedical applications [1], object recognition [2], polarization-encoded quantum key distribution [3], and polarization optical mapping [4]. A figure of merit of the linearly polarized photodetection is the degree of linear polarization (DOLP), where DOLP = $(I_{max} - I_{min})/(I_{max} + I_{min})$, where I_{max} and I_{min} are the photocurrents of the detected light parallel and perpendicular to the primary polarization direction, respectively. To date, high DOLP exceeding 0.9 has been reported for one-dimensional (1D) nanowires and nanobelts including InP [5], ZnO [6], Sb_2S_3 [7] and $BaTiS_3$ [8] due to their macroscopic anisotropy. Despite these efforts, the aspect ratios of 1D materials limit the diversified device preparation and additional non-integrable polarizing filters or polarizers are bulky and of high losses in use. Nowadays, to realize the demand of miniaturized device of photodetection, photodetectors based on two-dimensional (2D) materials show great potential due to their atomic thickness and unique optoelectronic properties [9, 10].

2D materials have been widely used in the fields of photodetectors [11], solar cells [12], ultrafast photonics [13] and nonlinear optics [14]. Among these, molybdenum disulfide (MoS_2), a typical 2D transition metal dichalcogenide (TMDC), was regarded as an ideal material for the next-generation high performance photodetectors due to its excellent electronic and optical properties such as wide wavelength absorption, direct bandgap in the monolayer, high power conversion efficiencies and high carrier mobility [15, 16]. Although the MoS_2-based photodetector achieved good performances, its intrinsic isotropy crystal and optical properties limited the application in polarization-sensitive photodetectors. Several intrinsic anisotropic 2D materials, for example, $ReSe_2$ [17], SnS [18], GeSe [19] and BP [20], have been widely used in polarization photodetectors for their anisotropic crystal and optical properties. However, the resonance wavelength and DOLP of these polarization-sensitive photodetectors using these anisotropy materials are still limited by their intrinsic properties, which limits the possibility of their applications. In these cases, it is still necessary to realize high polarization-sensitive photodetection with isotropy materials.

Gap-surface-plasmon (GSP) resonance can localize the light field and thus enhance the light absorption. It has been widely used in photodetectors for it can increase the photoresponsivity

Address correspondence to Xin Huang, xinhuang@iphy.ac.cn; Changzhi Gu, czgu@iphy.ac.cn

and extend operating wavelength [21–23]. Besides this, anisotropic nanostructures have been used to detect the polarization of light in isotropic 2D materials-based photodetectors. Chen et al. demonstrated a polarization modulator constructed by graphene and anisotropic Au nanostructure, which can detect the polarization state of light [24]. Wang et al. fabricated suspending WSe_2 flakes onto sub-20-nm-wide trenches in Au substrate and they demonstrated a polarization-dependent photoluminescence (PL) enhancement of 20,000-fold by Purcell factor of plasmonic nanostructure [25]. These researches show that linear polarization detection can be realized by introducing anisotropic metal nanostructure into 2D material devices.

In this work, a high polarization-sensitive photodetector composed of monolayer MoS_2 integrated with plasmonic nanocavity was demonstrated by using anisotropic plasmonic nanostructure to manipulate polarized light. The resonance mode of GSP was designed to match the neutral A-exciton wavelength of monolayer MoS_2. The Au nanogroove (NG) array was integrated at the bottom of the monolayer MoS_2. By doing this, the incident light polarized perpendicularly to the NG can be strongly confined due to the strong light confinement of GSP excitation. Furthermore, we demonstrate that the strong optical anisotropy introduced by the Au NG plasmonic nanocavity can be used to fabricate polarization-sensitive photodetectors, demonstrating a high photoresponsivity of 1.88 A/W and DOLP of 0.8 at an excitation wavelength of 633 nm. These results demonstrate that linearly polarized photodetection can be realized in the common 2D materials by coupling anisotropy plasmonic nanocavity. The fabrication technique for MoS_2 polarization-sensitive photodetectors could be applied to other isotropic and anisotropic 2D materials.

2 Results and discussion

The schematic of linear polarization-sensitive photodetector, consisting of MoS_2 monolayer and Au NG array, is shown in Fig. 1(a). The operating principle of photodetector shows that the GSP can be excited under incident light and the intensity of excited GSP reaches a maximum with the polarization direction of light perpendicular to NG (θ = 90°). The anisotropic localized electric field generated by GSP can modulate the interaction between monolayer MoS_2 and incident light. Figure 1(b) shows the optical microscope (OM) image of prepared MoS_2 photodetector, whose left part is MoS_2 with Au NG and right part is MoS_2 with unpatterned Au pad. This sample enables a direct comparison of device performance from the same single crystal MoS_2 flake, where the region over unpatterned Au pad is taken as the base reference. The monolayer MoS_2 (shown in Fig. S1 in the Electronic Supplementary Material (ESM)) was exfoliated from the bulk and transferred onto the prepared Au NG by the standard polydimethylsiloxane (PDMS) dry transfer method [26]. Figure 1(c) shows the Raman spectrum of monolayer MoS_2. Two specific Raman peaks at 384.3 cm^{-1} (E^1_{2g} mode) and 403 cm^{-1} (A_{1g} mode) can be seen, which can be attributed to the in-plane and out of plane modes. Figure 1(d) depicts the side view of scanning electron microscopy (SEM) images of Au NG nanostructure. The 200-nm Au pad was evaporated on Si/SiO_2 substrate by electron beam evaporation. The Au NG was fabricated by focused ion beam (FIB) milling on the fabricated Au pad and the V-shaped Au NG can be used to create the GSP mode with the light polarized perpendicularly to the NG [27]. The resonant wavelength of Au NG can be controlled by changing the depth of NG, which will be discussed in the following part. In order to avoid charge transfer between the MoS_2 and bottom Au substrate, an Al_2O_3 spacer film was deposited on the Au NG by atomic layer deposition before MoS_2 transfer. The profile of electric field was simulated by the finite element method (FEM) (Wave Optics module of COMSOL 5.5a). As shown in Fig. 1(e), the localized electric field of Au NG is parallel to the in-plane exciton dipoles of monolayer MoS_2, allowing to achieve the strong near-field enhancement by Purcell effect.

The key for preparing a high-performance polarization-sensitive photodetector is to optimize the shape of plasmonic nanocavity. In this case, the resonant wavelength of Au NG can be turned by controlling the depth of NG. Figure 2(a) shows measured reflectance spectra of Au NG with different depths of

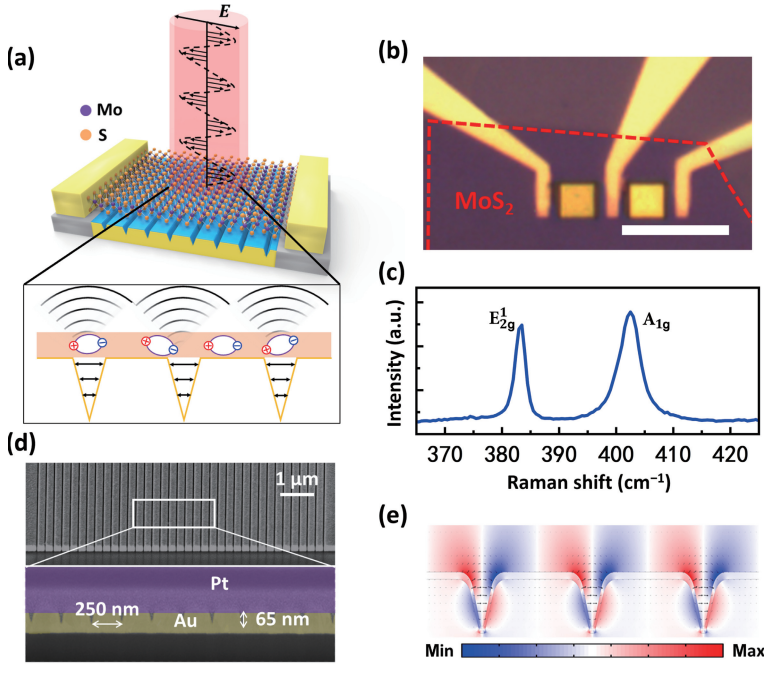

Figure 1 (a) Schematic of the hybrid structure of MoS_2 polarization photodetector with Au NG array. (b) Optical microscopy image of the designed MoS_2 photodetector where the left part is the MoS_2 with Au NG and right part is the MoS_2 with unpatterned Au pad. The scale bar is 10 μm. (c) Raman spectrum of the monolayer MoS_2, showing the E^1_{2g} and A_{1g} modes. (d) SEM images of designed Au NG array structure. (e) Finite-difference time-domain (FDTD) simulations for the distribution of electrical field intensity in NG.

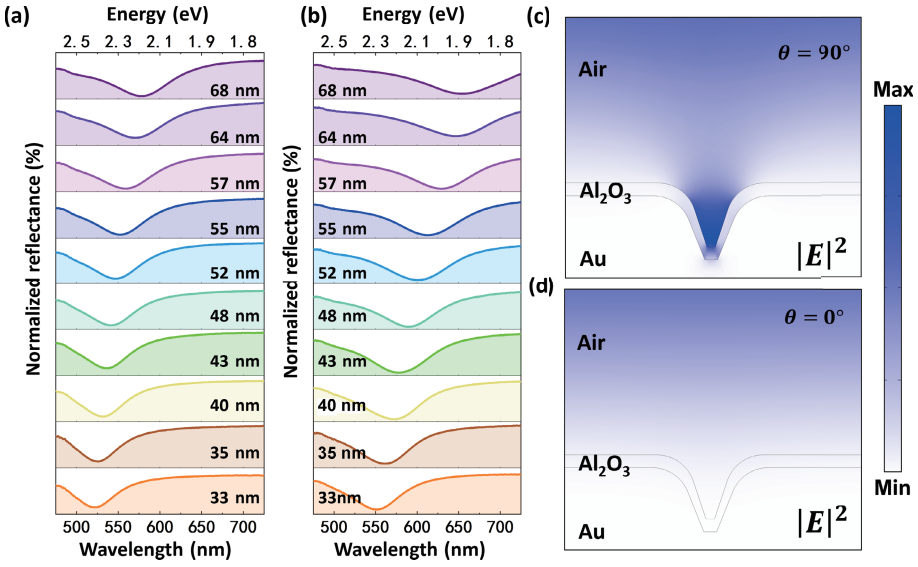

Figure 2 (a) The reflectance spectra of the Au NG array. The plasmonic resonance can be turned from 520 to 580 nm with the depth from 33 to 68 nm. (b) The reflectance spectra of the Au NG array with 10-nm Al_2O_3 deposited. The plasmonic resonances can be turned from 550 to 650 nm with the depth from 33 to 68 nm. The electric field distribution with (c) $\theta = 90°$ and (d) $\theta = 0°$.

NG from 33 to 68 nm. The pitch size of NG was fixed at 250 nm and the reflectance measurements were conducted with the polarization direction of light perpendicular to NG. The high absorption is attributed to a strongly enhanced field around the opening of NG. The plasmonic resonance of Au NG has a red shift of 30–70 nm following deposition of 10 nm Al_2O_3 (refractive index of Al_2O_3 is 1.76), as shown in Fig. 2(b). The simulated reflectance spectra shown in Fig. S2 in the ESM were also calculated by changing the depth of NG. The calculated reflectance spectra are in good agreement with experimental results. It can be seen clearly that the resonant wavelength of Au NG can be changed from 520 to 580 nm with the depth from 33 to 58 nm, exhibiting a linear relationship with the NG depth, as shown in Fig. S3(a) in the ESM. The incident laser polarization angle is defined as θ. For the NG structure, the light absorption is maximized when the electric field of the incident light is polarized perpendicular to the NG (θ = 90°), and reduced when the electric field is polarized parallel to the NG (θ = 0°). The electric field intensity $|E|^2$ of Au NG shown in Figs. 2(c) and 2(d) was calculated under 633 nm light irradiation with various polarized angles θ. It can be observed that the electric field intensity under θ = 90° is stronger than that under θ = 0°, which leads to largest absorption with incident light polarized perpendicular to the NG. With the polarization-dependent GSP resonance, the intensity of near-field can be adjusted by polarization of the incident light, which is the key to achieving an MoS_2-based polarization-sensitive photodetector.

Figure 3 presents comparisons of reflectance and PL spectra from MoS_2 on NG with depths of 50, 75 and 95 nm, respectively. The relative reflectance spectra measured from Au NG before and after MoS_2 transfer, which were normalized to the reflectance spectra from the unpatterned Au pad. As summarized in Fig. 3, the plasmon resonance of individual Au NG red-shifts after covering with monolayer MoS_2. Moreover, The PL spectra were measured using a 633 nm pump laser with a power of 1 μW. The PL enhancement factor is defined as $\lambda = I(\theta = 90°)/I(SiO_2$ substrate), where $I(\theta)$ indicates the integrated PL intensity of MoS_2-Au NG coupled system excited by the laser with polarized angle of θ and $I(SiO_2$ substrate) the integrated PL intensity of MoS_2 on SiO_2 substrate excited by the laser. The sample with 50-nm-depth NG reaches a maximum 24-fold enhancement of PL emission (Fig. 3(b)) as compared with 12-fold and 4-fold PL enhancement from 75-nm (Fig. 3(e)) and 95-nm-depth NG (Fig. 3(h)), respectively. The peak position of the PL spectrum red-shifts, and the linewidth of the spectrum is broadened in MoS_2-Au NG hybrid structure as shown in Fig. 3(b). The emission peak red-shifts from 1.87 to 1.81 eV and the width shifts from 84 to 114 meV. Broadening and red-shift of PL emission can be attributed to the coupling of excitons in monolayer MoS_2 with gap plasmon [28]. This phenomenon can also be induced by the complex interaction between Au NG and MoS_2 such as local doping, strain, etc. [29–31]. Moreover, the PL intensity of monolayer MoS_2 on bare Au pad is enhanced slightly compared with that on SiO_2 substrate, which might be considered as the multi-scattering of light between Au and MoS_2 interfaces [32].

Considering the physical processes involved in the PL measurement, the PL intensity of emitters is determined by its excitation rate and emission efficiency. In this work, the enhancement of excitation rate of MoS_2 depends on the match between plasmon resonance of MoS_2-Au NG structure and the wavelength of the pump laser, that is, $\gamma_{exc} \propto |E_{NF}|^2$, where γ_{exc} and E_{NF} denote excitation rate and near-field intensity enhancement respectively [33]. Otherwise, the emission efficiency increase for the nonradiative decay rate is suppressed by the plasmonic resonances, thus enhancing the quantum efficiency via the Purcell effect. Therefore, the largest PL enhancement occurs when the exciton wavelength matches the plasmon resonance. Under the irradiation of a 633-nm pump laser, the plasmonic resonant wavelength of 50-nm-depth NG is close to the laser wavelength, and the strong excitation of GSP resonance can be excited to effectively promote the near-field enhancement and quantum efficiency to improve the light absorption and generation of electron–hole pairs in MoS_2. The distribution of near-field intensity of MoS_2-Au NG structure was simulated and the near-field intensity becomes more pronounced for the case of 50-nm-depth NG as shown in Fig. 3(c). Figure S4(a) in the ESM presents the corresponding PL spectra as excited by 532-nm pump laser. Excitation at 532 nm results in low near-filed enhancement and low PL enhancements, which can be attributed to the mismatch between plasmonic resonance and incident wavelength. Figure S4(b) in the ESM shows that the PL spectrum of the MoS_2 on unpatterned Au pad is almost consistent with the one with incident laser parallel to NG (θ = 0°) and does not change with θ, demonstrating that bare MoS_2 is not sensitive to incident light

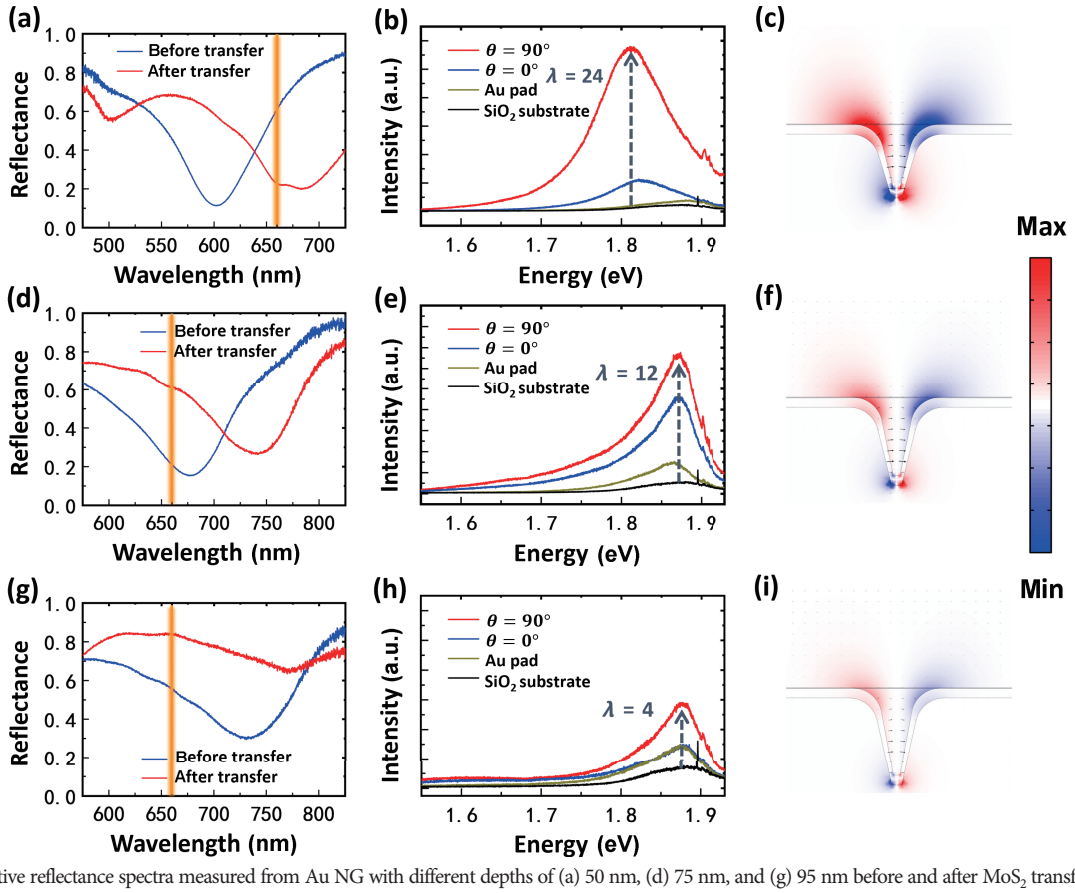

Figure 3 Relative reflectance spectra measured from Au NG with different depths of (a) 50 nm, (d) 75 nm, and (g) 95 nm before and after MoS_2 transfer. PL intensity enhancement of monolayer MoS_2 on Au NG with different depths of (b) 50 nm, (e) 75 nm, and (h) 95 nm excited by the 633 nm laser. The simulated distribution of electric field intensity with different depths of Au NG: (c) 50 nm, (f) 75 nm, and (i) 95 nm.

polarization with both 532 and 633-nm pump lasers. The MoS_2 crystal direction didn't deliberately align with Au NG, and therefore the polarization response in this MoS_2 device can be induced by the plasmon resonance.

The enhancement quantum efficiency will generate more electron–hole pairs and the anisotropic optical properties will promote linear polarization-sensitive photodetection in the MoS_2-Au NG coupled systems. The photocurrent ΔI_{ph} ($\Delta I_{ph} = I_{ph} - I_{dark}$) measurements were performed under illumination of a 633 nm pump laser with different polarization angles (θ). The curves of photocurrent ΔI_{ph} vs. source-drain bias V_d at the incident laser powers of 0.1 and 1 μW are demonstrated in Figs. 4(a) and 4(b) respectively. We can clearly see that as the polarization angle θ is increased from 0° to 90° with the laser power of 0.1 μW, the ΔI_{ph} gradually increase from 0.026 to 0.188 μA. The increased ΔI_{ph} was caused by increasing absorption and quantum efficiency due to the plasmonic resonance. These results indicate a high photoresponsivity 1.88 A/W and polarization sensitivity of MoS_2 photodetector. In order to verify that the polarization sensitivity of MoS_2 photodetectors is induced by the anisotropic plasmonic effect of Au NG, the photocurrent characteristics of MoS_2 on the unpatterned Au pad on SiO_2 substrate were also presented. With the laser power up to 1 μW, the photoresponsivity decreases to 0.36 A/W, which is a common behavior of photodetectors due to saturation of electron–hole pair generation at a high laser power and the increased surface recombination [23]. Figure 4(c) shows the DOLP results as a function of V_d and we can achieve a high DOLP of 0.8 at a laser power of 0.1 μW. Figure 4(d) displays a comparison of DOLP results for devices with different GSP resonant wavelengths. The DOLP gradually decreases with the increasing resonance wavelength of NG, which is in good agreement with the previous PL results and the simulated near-field enhancement. The photocurrent–time curves (ΔI_{ph}–t) for MoS_2 photodetector under a bias of 5 V are shown in Fig. 4(e). Under the illumination of 633 nm laser, the photocurrent of the device rapidly rises to a stable value and decays fast after removal of the light. It demonstrates that these devices have a good photo switching behavior and good stability during the temporary on/off test.

The earlier studies show that the DOLPs of most 2D-materials based polarization-sensitive photodetectors are within the value of 0.7 and the response wavelengths are in the range of 300–900 nm, as shown in Fig. 5 [17, 19, 34–46]. In contrast, we have achieved a larger DOLP compared to the previous works based on 1D and 2D coupled systems due to large electromagnetic field confinement provided by Au NG structure. Although a higher DOLP achieved from mixed-dimensional system based on graphene/$PdSe_2$/Ge heterojunction, the complex preparation process limits its application. Given high stability and polarization sensitivity, the design of plasmonic nanocavity-enhanced MoS_2 photodetector devices holds promise for high-performance polarization-sensitive broadband photodetection.

3 Conclusion

In summary, high-performance polarization-sensitive detectors were designed by integrating monolayer MoS_2 with anisotropic plasmonic nanocavity. The localized electric field generated by Au NG can enhance the light absorption and quantum efficiency of monolayer MoS_2. The anisotropy optical properties also provide a feasible and effective solution to realize polarization-sensitive photodetection on MoS_2 photodetectors. Our results indicate that Au NG can be used to realize linear polarization photodetection in MoS_2 photodetector, with the photoresponsivity reaching 1.88 A/W and DOLP of 0.8 at the excitation wavelength of 633 nm.

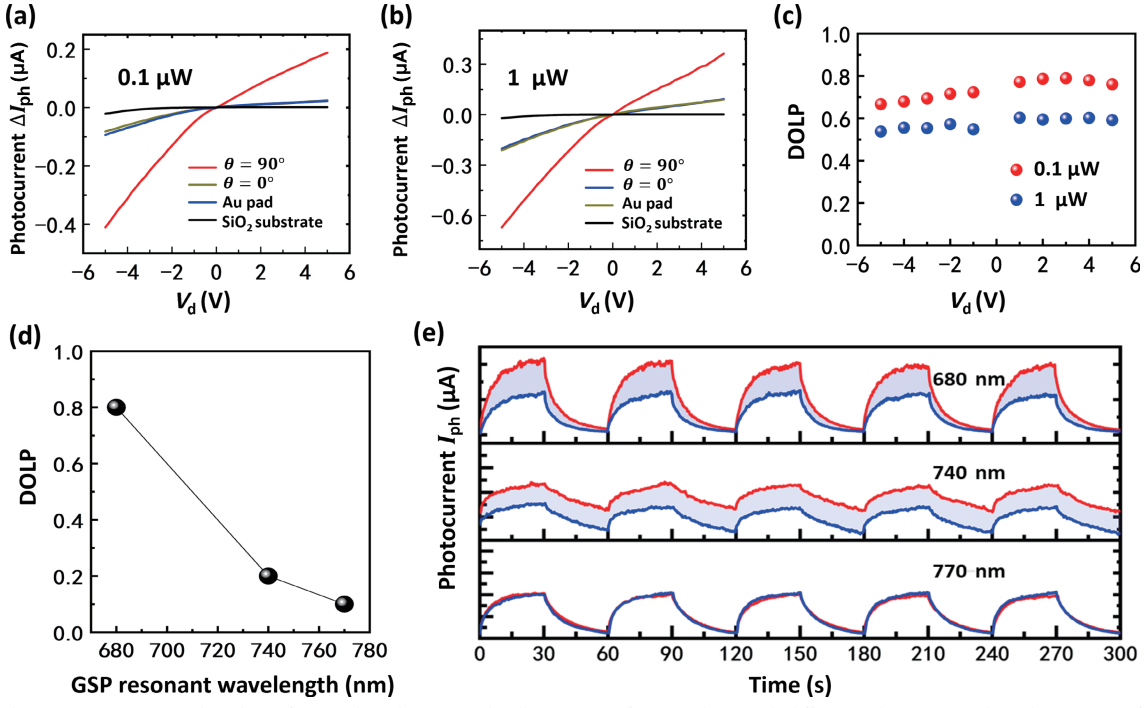

Figure 4 Photocurrent vs. source-drain bias of MoS_2 photodetector under illumination of 633 nm laser, with different polarization angles at laser power of (a) 0.1 μW and (b) 1 μW. (c) DOLP vs. bias voltage for 633 nm incident laser with both 0.1 and 1 μW power. (d) Comparison of DOLPs with different resonance wavelengths. (e) Time-dependent photocurrent response curves (ΔI_{ph}–t) of two perpendicular directions of incident light by a 633 nm laser with 1 μW power.

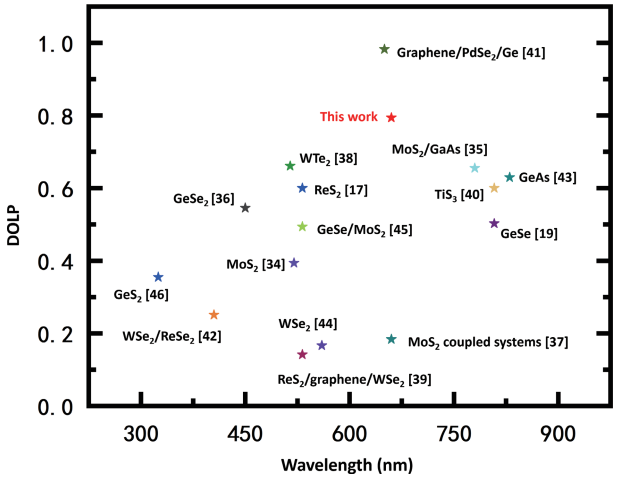

Figure 5 Comparison of DOLP and corresponding response wavelength of anisotropic system-based polarization-sensitive photodetectors.

Our results indicate a promising application of polarization-dependent plasmonic manipulation in isotropic two-dimension semiconductor materials and devices.

4 Methods

4.1 Device fabrication

A thick Au pad of 200 nm was deposited on Si/SiO_2 substrate using an electron-gun evaporation system (Peva-600E). The Au NG was then milled using a FIB system (Helios 600i, FEI) under an acceleration voltage of 30 kV and an ion beam current of 7.7 pA. Then, e-beam lithography (EBL) was carried out to define the electrodes and Au was electron-beam-evaporated onto the sample followed with lift-off process. MoS_2 monolayers were mechanically exfoliated from bulk MoS_2 crystals. The MoS_2 coupled Au NG systems were prepared with PDMS stamp by a dry-transfer technique.

4.2 Experimental measurement

For white light spectral measurement, a confocal microscope (WITec Alpha 300R) with a halogen lamp was used to measure the reflectance of samples. A 100× objective lens (Olympus) with a numerical aperture (NA) of 0.9 was used to collect the reflectance signal. Polarization of the incident white light was controlled by placing a broadband polarizer between the white light source and the sample. During Raman and PL measurement, the samples were excited using 633 and 532 nm lasers at 1 μW to avoid sample damage. The Raman and PL signals were collected using a 100× objective lens with an NA of 0.9. The polarization orientation of the incident laser was fixed, and the angle parallel/perpendicular to the long axis of the NG array was realized by rotating the sample. For photocurrent measurements, a sourcemeter (Keithley 2450 series) was used for different kinds of measurements.

Acknowledgements

This work was supported by the National Key Research and Development Program of China (No. 2021YFA1400700), the National Natural Science Foundation of China (Nos. 61888102, 62204259, 62174179, 92265110, 11974386, 12074420, U21A20140 and 61905274), the Beijing Municipal Science & Technology Commission, Administrative Commission of Zhongguancun Science Park (No. Z211100004821009), the Strategic Priority Research Program of Chinese Academy of Sciences (CAS) (Nos. XDB33000000 and XDB28000000), the Key Research Program of Frontier Sciences of CAS (Nos. QYZDJ-SSWSLH042 and XDPB22). and the Project for Young Scientists in Basic Research of CAS (No. YSBR021). This work was also supported by the Synergic Extreme Condition User Facility, China.

Electronic Supplementary Material: Supplementary material (further details of the Raman spectra, AFM image, calculated reflectance spectra, and additional data) is available in the online version of this article at https://doi.org/10.1007/s12274-023-5724-9.

References

[1] Baumann, B.; Harper, D. J.; Eugui, P.; Gesperger, J.; Lichtenegger, A.; Merkle, C. W.; Augustin, M.; Woehrer, A. Improved accuracy of quantitative birefringence imaging by polarization sensitive OCT with simple noise correction and its application to neuroimaging. *J. Biophotonics* **2021**, *14*, e202000323.

[2] Li, N.; Zhao, Y. Q.; Pan, Q.; Kong, S. G.; Chan, J. C. W. Illumination-invariant road detection and tracking using LWIR polarization characteristics. *ISPRS J. Photogramm. Remote Sens.* **2021**, *180*, 357–369.

[3] Ye, T. Y.; Li, H. K.; Hu, J. L. Information leakage resistant quantum dialogue with single photons in both polarization and spatial-mode degrees of freedom. *Quantum Inf. Process.* **2021**, *20*, 209.

[4] Kim, S.; Cense, B.; Joo, C. Single-pixel, single-input-state polarization-sensitive wavefront imaging. *Opt. Lett.* **2020**, *45*, 3965–3968.

[5] Wang, J. F.; Gudiksen, M. S.; Duan, X. F.; Cui, Y.; Lieber, C. M. Highly polarized photoluminescence and photodetection from single indium phosphide nanowires. *Science* **2001**, *293*, 1455–1457.

[6] Soci, C.; Zhang, A.; Xiang, B.; Dayeh, S. A.; Aplin, D. P. R.; Park, J.; Bao, X. Y.; Lo, Y. H.; Wang, D. ZnO nanowire UV photodetectors with high internal gain. *Nano Lett.* **2007**, *7*, 1003–1009.

[7] Zhong, M. Z.; Wang, X. H.; Liu, S. J.; Li, B.; Huang, L.; Cui, Y.; Li, J. B.; Wei, Z. M. High-performance photodetectors based on Sb_2S_3 nanowires: Wavelength dependence and wide temperature range utilization. *Nanoscale* **2017**, *9*, 12364–12371.

[8] Niu, S. Y.; Joe, G.; Zhao, H.; Zhou, Y. C.; Orvis, T.; Huyan, H. X.; Salman, J.; Mahalingam, K.; Urwin, B.; Wu, J. B. et al. Giant optical anisotropy in a quasi-one-dimensional crystal. *Nat. Photonics* **2018**, *12*, 392–396.

[9] Nasiri, N.; Jin, D. Y.; Tricoli, A. Nanoarchitechtonics of visible-blind ultraviolet photodetector materials: Critical features and nano-microfabrication. *Adv. Opt. Mater.* **2019**, *7*, 1800580.

[10] Yu, Y.; Wang, W. Y.; Li, W. H.; Wang, G.; Wang, Y. L.; Lu, Z. W.; Li, S. S.; Zhao, W. L.; Li, Y. H.; Liu, T. Y. et al. Photodetectors based on micro-nano structure material. *Front. Chem.* **2022**, *9*, 832028.

[11] Mak, K. F.; Shan, J. Photonics and optoelectronics of 2D semiconductor transition metal dichalcogenides. *Nat. Photonics* **2016**, *10*, 216–226.

[12] Buscema, M.; Island, J. O.; Groenendijk, D. J.; Blanter, S. I.; Steele, G. A.; van der Zant, H. S. J.; Castellanos-Gomez, A. Photocurrent generation with two-dimensional van der Waals semiconductors. *Chem. Soc. Rev.* **2015**, *44*, 3691–3718.

[13] Hong, X. P.; Kim, J.; Shi, S. F.; Zhang, Y.; Jin, C. H.; Sun, Y. H.; Tongay, S.; Wu, J. Q.; Zhang, Y. F.; Wang, F. Ultrafast charge transfer in atomically thin MoS_2/WS_2 heterostructures. *Nat. Nanotechnol.* **2014**, *9*, 682–686.

[14] Liu, X. Z.; Yi, J.; Yang, S.; Lin, E. C.; Zhang, Y. J.; Zhang, P. Y.; Li, J. F.; Wang, Y.; Lee, Y. H.; Tian, Z. Q. et al. Nonlinear valley phonon scattering under the strong coupling regime. *Nat. Mater.* **2021**, *20*, 1210–1215.

[15] Radisavljevic, B.; Radenovic, A.; Brivio, J.; Giacometti, V.; Kis, A. Single-layer MoS_2 transistors. *Nat. Nanotechnol.* **2011**, *6*, 147–150.

[16] Mak, K. F.; Lee, C.; Hone, J.; Shan, J.; Heinz, T. F. Atomically thin MoS_2: A new direct-gap semiconductor. *Phys. Rev. Lett.* **2010**, *105*, 136805.

[17] Liu, F. C.; Zheng, S. J.; He, X. X.; Chaturvedi, A.; He, J. F.; Chow, W. L.; Mion, T. R.; Wang, X. L.; Zhou, J. D.; Fu, Q. D. et al. Highly sensitive detection of polarized light using anisotropic 2D ReS_2. *Adv. Funct. Mater.* **2016**, *26*, 1169–1177.

[18] Cui, Y.; Zhou, Z. Q.; Wang, X. H.; Wang, X. T.; Ren, Z. H.; Pan, L. F.; Yang, J. H. Wavelength-selectivity polarization dependence of optical absorption and photoresponse in SnS nanosheets. *Nano Res.* **2021**, *14*, 2224–2230.

[19] Wang, X. T.; Li, Y. T.; Huang, L.; Jiang, X. W.; Jiang, L.; Dong, H. L.; Wei, Z. M.; Li, J. B.; Hu, W. P. Short-wave near-infrared linear dichroism of two-dimensional germanium selenide. *J. Am. Chem. Soc.* **2017**, *139*, 14976–14982.

[20] Yuan, H. T.; Liu, X. G.; Afshinmanesh, F.; Li, W.; Xu, G.; Sun, J.; Lian, B.; Curto, A. G.; Ye, G. J.; Hikita, Y. et al. Polarization-sensitive broadband photodetector using a black phosphorus vertical p-n junction. *Nat. Nanotechnol.* **2015**, *10*, 707–713.

[21] Du, B. W.; Yang, W. Q.; Jiang, Q.; Shan, H. Y.; Luo, D. Y.; Li, B. W.; Tang, W. C.; Lin, F.; Shen, B.; Gong, Q. H. et al. Plasmonic-functionalized broadband perovskite photodetector. *Adv. Opt. Mater.* **2018**, *6*, 1701271.

[22] Dai, M. J.; Chen, H. Y.; Feng, R.; Feng, W.; Hu, Y. X.; Yang, H. H.; Liu, G. B.; Chen, X. S.; Zhang, J.; Xu, C. Y. et al. A dual-band multilayer InSe self-powered photodetector with high performance induced by surface Plasmon resonance and asymmetric schottky junction. *ACS Nano* **2018**, *12*, 8739–8747.

[23] Wu, Z. Q.; Yang, J. L.; Manjunath, N. K.; Zhang, Y. J.; Feng, S. R.; Lu, Y. H.; Wu, J. H.; Zhao, W. W.; Qiu, C. Y.; Li, J. F. et al. Gap-mode surface-plasmon-enhanced photoluminescence and photo-response of MoS_2. *Adv. Mater.* **2018**, *30*, 1706527.

[24] Li, J. X.; Yu, P.; Cheng, H.; Liu, W. W.; Li, Z. C.; Xie, B. Y.; Chen, S. Q.; Tian, J. G. Optical polarization encoding using graphene-loaded plasmonic metasurfaces. *Adv. Opt. Mater.* **2016**, *4*, 91–98.

[25] Wang, Z.; Dong, Z. G.; Gu, Y. H.; Chang, Y. H.; Zhang, L.; Li, L. J.; Zhao, W. J.; Eda, G.; Zhang, W. J.; Grinblat, G. et al. Giant photoluminescence enhancement in tungsten-diselenide-gold plasmonic hybrid structures. *Nat. Commun.* **2016**, *7*, 11283.

[26] Splendiani, A.; Sun, L.; Zhang, Y. B.; Li, T. S.; Kim, J.; Chim, C. Y.; Galli, G.; Wang, F. Emerging photoluminescence in monolayer MoS_2. *Nano Lett.* **2010**, *10*, 1271–1275.

[27] Smith, C. L. C.; Stenger, N.; Kristensen, A.; Mortensen, N. A.; Bozhevolnyi, S. I. Gap and channeled plasmons in tapered grooves: A review. *Nanoscale* **2015**, *7*, 9355–9386.

[28] Park, Y.; Han, S. W.; Chan, C. C. S.; Reid, B. P. L.; Taylor, R. A.; Kim, N.; Jo, Y.; Im, H.; Kim, K. S. Interplay between many body effects and Coulomb screening in the optical bandgap of atomically thin MoS_2. *Nanoscale* **2017**, *9*, 10647–10652.

[29] Kim, H.; Im, J.; Nam, K.; Han, G. H.; Park, J. Y.; Yoo, S.; Haddadnezhad, M.; Park, S.; Park, W.; Ahn, J. S. et al. Plasmon-exciton couplings in the MoS_2/AuNP plasmonic hybrid structure. *Sci. Rep.* **2022**, *12*, 22252.

[30] Huang, J. N.; Akselrod, G. M.; Ming, T.; Kong, J.; Mikkelsen, M. H. Tailored emission spectrum of 2D semiconductors using plasmonic nanocavities. *ACS Photonics* **2018**, *5*, 552–558.

[31] Li, Z. W.; Lv, Y. W.; Ren, L. W.; Li, J.; Kong, L. G.; Zeng, Y. J.; Tao, Q. Y.; Wu, R. X.; Ma, H. F.; Zhao, B. et al. Efficient strain modulation of 2D materials via polymer encapsulation. *Nat. Commun.* **2020**, *11*, 1151.

[32] Huang, X.; Feng, X. W.; Chen, L.; Wang, L.; Tan, W. C.; Huang, L.; Ang, K. W. Fabry-Perot cavity enhanced light-matter interactions in two-dimensional van der Waals heterostructure. *Nano Energy* **2019**, *62*, 667–673.

[33] Wientjes, E.; Renger, J.; Curto, A. G.; Cogdell, R.; van Hulst, N. F. Strong antenna-enhanced fluorescence of a single light-harvesting complex shows photon antibunching. *Nat. Commun.* **2014**, *5*, 4236.

[34] Tong, L.; Duan, X. Y.; Song, L. Y.; Liu, T. D.; Ye, L.; Huang, X. Y.; Wang, P.; Sun, Y. H.; He, X.; Zhang, L. J. et al. Artificial control of in-plane anisotropic photoelectricity in monolayer MoS_2. *Appl. Mater. Today* **2019**, *15*, 203–211.

[35] Jia, C.; Wu, D.; Wu, E. P.; Guo, J. W.; Zhao, Z. H.; Shi, Z. F.; Xu, T. T.; Huang, X. W.; Tian, Y. T.; Li, X. J. A self-powered high-performance photodetector based on a MoS_2/GaAs heterojunction with high polarization sensitivity. *J. Mater. Chem. C* **2019**, *7*, 3817–3821.

[36] Yang, Y. S.; Liu, S. C.; Yang, W.; Li, Z. B.; Wang, Y.; Wang, X.; Zhang, S. S.; Zhang, Y.; Long, M. S.; Zhang, G. M. et al. Air-stable in-plane anisotropic $GeSe_2$ for highly polarization-sensitive photodetection in short wave region. *J. Am. Chem. Soc.* **2018**, *140*, 4150–4156.

[37] Chen, S.; Cao, R.; Chen, X.; Wu, Q.; Zeng, Y. H.; Gao, S.; Guo, Z. N.; Zhao, J. L.; Zhang, M.; Zhang, H. Anisotropic plasmonic nanostructure induced polarization photoresponse for MoS_2-based photodetector. *Adv. Mater. Interfaces* **2020**, *7*, 1902179.

[38] Zhou, W.; Chen, J. Z.; Gao, H.; Hu, T.; Ruan, S. C.; Stroppa, A.;

Ren, W. Anomalous and polarization-sensitive photoresponse of T_d-WTe_2 from visible to infrared light. *Adv. Mater.* **2019**, *31*, 1804629.

[39] Wang, Z. D.; Zeng, P. Y.; Hu, S. J.; Wu, X. M.; He, J. Y.; Wu, Z. T.; Wang, W. H.; Zheng, P.; Zheng, H.; Zheng, L. et al. Broadband photodetector based on ReS_2/graphene/WSe_2 heterostructure. *Nanotechnology* **2021**, *32*, 465201.

[40] Liu, S. J.; Xiao, W. B.; Zhong, M. Z.; Pan, L. F.; Wang, X. T.; Deng, H. X.; Liu, J.; Li, J. B.; Wei, Z. M. Highly polarization sensitive photodetectors based on quasi-1D titanium trisulfide (TiS_3). *Nanotechnology* **2018**, *29*, 184002.

[41] Wu, D.; Guo, J. W.; Du, J.; Xia, C. X.; Zeng, L. H.; Tian, Y. Z.; Shi, Z. F.; Tian, Y. T.; Li, X. J.; Tsang, Y. H. et al. Highly polarization-sensitive, broadband, self-powered photodetector based on graphene/$PdSe_2$/germanium heterojunction. *ACS Nano* **2019**, *13*, 9907–9917.

[42] Ahn, J.; Ko, K.; Kyhm, J. H.; Ra, H. S.; Bae, H.; Hong, S.; Kim, D. Y.; Jang, J.; Kim, T. W.; Choi, S. et al. Near-infrared self-powered linearly polarized photodetection and digital incoherent holography using WSe_2/$ReSe_2$ van der Waals heterostructure. *ACS Nano* **2021**, *15*, 17917–17925.

[43] Zhou, Z. Q.; Long, M. S.; Pan, L. F.; Wang, X. T.; Zhong, M. Z.; Blei, M.; Wang, J. L.; Fang, J. Z.; Tongay, S.; Hu, W. D. et al. Perpendicular optical reversal of the linear dichroism and polarized photodetection in 2D GeAs. *ACS Nano* **2018**, *12*, 12416–12423.

[44] Guskov, A.; Lavrov, S.; Galiev, R. Polarization sensitive photodetectors based on two-dimensional WSe_2. *Nanomaterials* **2022**, *12*, 1854.

[45] Xin, Y.; Wang, X. X.; Chen, Z.; Weller, D.; Wang, Y. Y.; Shi, L. J.; Ma, X.; Ding, C. J.; Li, W.; Guo, S. et al. Polarization-sensitive self-powered type-II GeSe/MoS_2 van der Waals heterojunction photodetector. *ACS Appl. Mater. Interfaces* **2020**, *12*, 15406–15413.

[46] Yang, Y. S.; Liu, S. C.; Wang, X.; Li, Z. B.; Zhang, Y.; Zhang, G. M.; Xue, D. J.; Hu, J. S. Polarization-sensitive ultraviolet photodetection of anisotropic 2D GeS_2. *Adv. Funct. Mater.* **2019**, *29*, 1900411.